Varied CO_2 photoreduction activity over UiO-66-NH_2 with different morphology

Shu-Ran Zhang[a,b], Yan-Hong Zou[c], Hai-Ning Wang*[c], Guang-Juan Xu[a], Wei Xie[a], Na Xu[a], Yan-Hong Xu*[a] and Ya-Qian Lan*[d]

[a]*Key Laboratory of Preparation and Applications of Environmental Friendly Materials (Jilin Normal University), Ministry of Education, Changchun 130103, Jilin, People's Republic of China.*
[b]*The Joint Laboratory of Intelligent Manufacturing of Energy and Environmental Materials, Changchun, 130103, Jilin, People's Republic of China*
[c]*School of Chemistry and Chemical Engineering, Shandong University of Technology, Zibo 255049, People's Republic of China.*
[d]*School of Chemistry, National and Local Joint Engineering Research Center of MPTES in High Energy and Safety LIBs, Engineering Research Center of MTEES (Ministry of Education) Key Lab. of ETESPG(GHEI), South China Normal University Guangzhou, 510006 (P. R. China).*

Experimental Section

Chemicals

All used reagents and solvents are commercially available and used directly. Zirconium tetrachloride ($ZrCl_4$, 99.5%), 2-aminoterephthalic acid, Acetic acid glacial, Ethanol, 5% Nafion solution, *N,N*-Dimethyformamide (DMF), were purchased from Shanghai Macklin Biochemical Co., Ltd., China. All chemical reagents were used directly without any further purification. Ultrapure water was used throughout.

Instruments

Fourier transform infrared spectroscopy (FT-IR) spectra were recorded with a Thermo Nicolet 5700 by using KBr pellets for sample. X-ray powder diffraction patterns of the samples were recorded on a Bruker D8 Advance diffractometer with Cu KR (λ = 1.5418 Å) radiation in the range of 5–70°. The morphology analysis of the synthesized samples was collected on a scanning electron microscope (SEM, sirion200) at an acceleration voltage of 10 kV. UV-vis absorption spectrum was obtained on UV-2550 spectrophotometer (Shimadzu, Japan). Nitrogen adsorption-desorption isotherms and the CO_2 adsorption/desorption measurements were conducted under 77 K and the ambient condition of 298 K on BeiShiDe Instrument BSD-PS(M) respectively.

Synthesis and Preparations

Synthesis of BUiO-66-NH_2

BUiO-66-NH_2 was prepared according to the reported literature [S1].

Synthesis of AUiO-66-NH_2

AUiO-66-NH_2 was prepared according to the reported literature [S2].

Synthesis of UiO-66-NH_2

UiO-66-NH_2 was prepared according to the reported literature [S3].

2.3 General Catalytic Reduction

2.3.1 Photocatalytic CO_2 reduction

Photocatalyst (1 mg) was dispersed in 1 mL ethanol and then coated on 1 cm × 3 cm glass. The cover range is 1 cm × 3 cm. The prepared samples were placed in a self-made photocatalytic reactor, and 150 μL distilled water was added at the bottom as the reducing agent. CO_2 was introduced into the reactor to replace air and ensured that the reactor was full of CO_2. LED lamp was used as the light source. After irradiation for 2 hours, 0.5 mL and 1.0 mL gas were taken and placed in gas chromatography (GC 1120) to determine the content of CO and H_2.

2.3.2 CO_2 Photoreduction Analysis

The electrochemical analyzer (CHI 760E) was used for photoelectrochemical test and Motschottky test with the standard three electrode system. Sodium sulfate solution (0.2 mol/L) served as the electrolyte. The sample (1 mg) and 5% Nafion solution were added into 2 mL ethanol for 1 h, and then evenly dropped on a 1 cm × 2 cm ITO conductive glass as the working electrode. The reference electrode was the Ag/AgCl electrode and the counter electrode was the platinum electrode.

The thermal stability of three UiO-66-NH_2

The TG curves of three UiO-66-NH_2 have been performed, and given here, which show that all UiO-66-NH_2 achieve the great thermal stability and are stable up to about 200 °C.

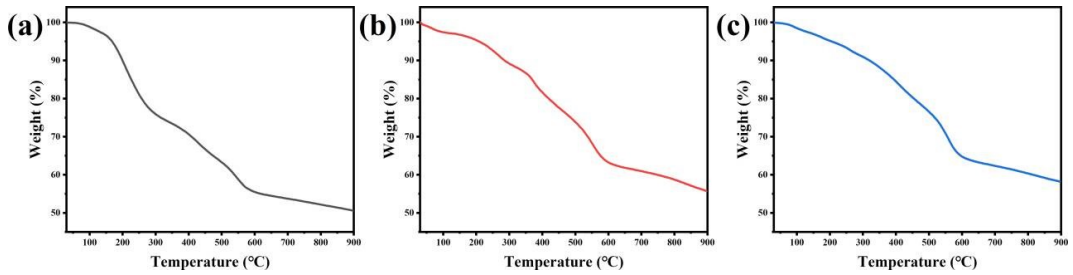

Fig. S1 The TG curves of BUiO-66-NH_2 (a), AUiO-66-NH_2 (b) and UiO-66-NH_2 (c).

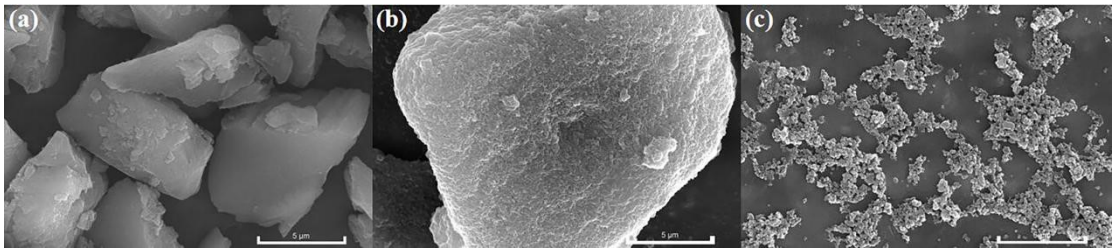

Fig. S2 The SEM images of (a) BUiO-66-NH_2, (b) AUiO-66-NH_2 and (c) UiO-66-NH_2.

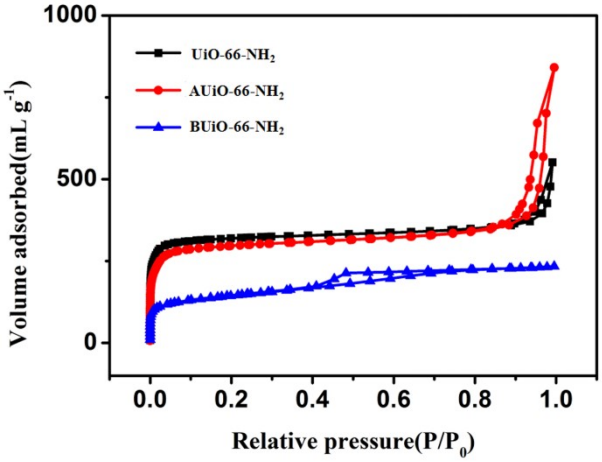

Fig. S3 The N_2 adsorption-desorption curves of BUiO-66-NH_2, AUiO-66-NH_2 and UiO-66-NH_2.

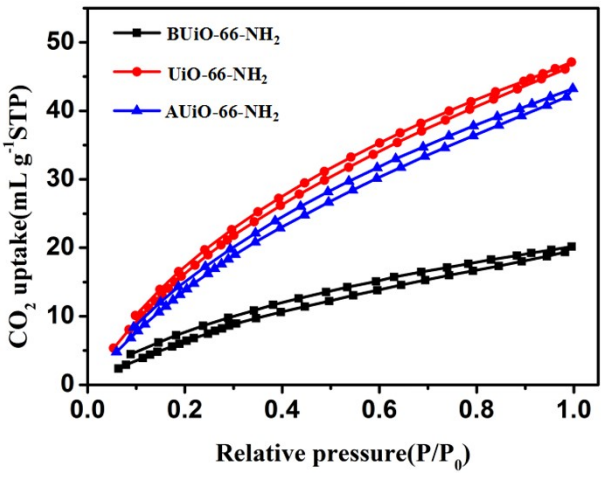

Fig. S4 The CO_2 absorption of BUiO-66-NH_2, AUiO-66-NH_2 and UiO-66-NH_2.

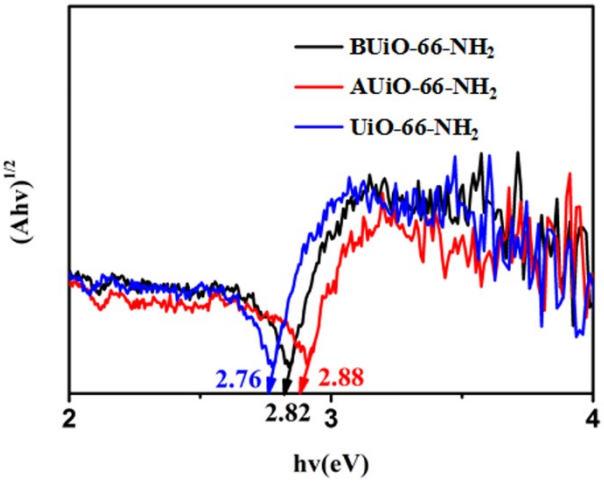

Fig. S5 The Tauc plots of BUiO-66-NH_2, AUiO-66-NH_2 and UiO-66-NH_2.

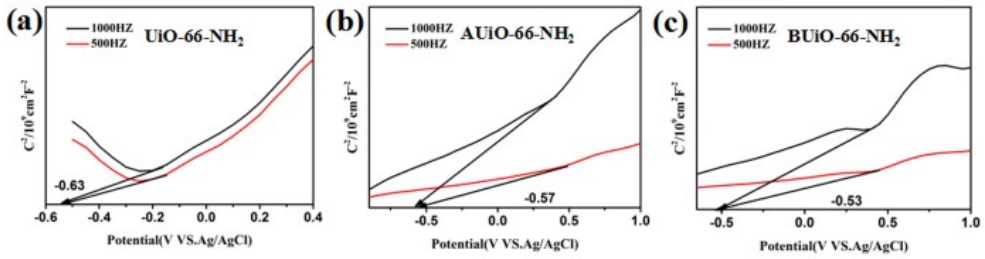

Fig. S6 The M-S plots of BUiO-66-NH_2, AUiO-66-NH_2 and UiO-66-NH_2.

Table S1 The performances of covered MOFs for CO_2 photoreduction.

Type	Sacrifice agent	The formation rate of CO (μmol g^{-1} h^{-1})	Ref.
UiO-66-NH_2	H_2O	69.3	This work
Bi-PMOF-120-F	TEOA	28.61	S4
NH_2-MIL-125(Ti)	TEOA	8.25	S5
Co-MOF	TEOA	27.1	S6
Ni-MOF NNs	TEOA	8.05	S7
$Co_{0.1}Ni_{0.9}$-MOF	H_2O	38.74	S8
Ni-Bpyb	TIPA	1326.7	S9
AQNU-5	TEA	56.2	S10
IHEP-101	H_2O	458	S11
Ni-MOF(H_2O)	TEOA	9610	S12
Co_1Ni_2-MOF	TEOA	1160	S13
Zn/Co/Mo-MOF	TEOA	38.41	S14
Co-Fe PBA	TEOA	14.49	S15
PCN-601	H_2O	6	S16
MAF-34-CoRu	H_2O	11.2	S17
MOF-74	H_2O	1.484	S18
MIL-101-Cr	TEOA	8.3	S19

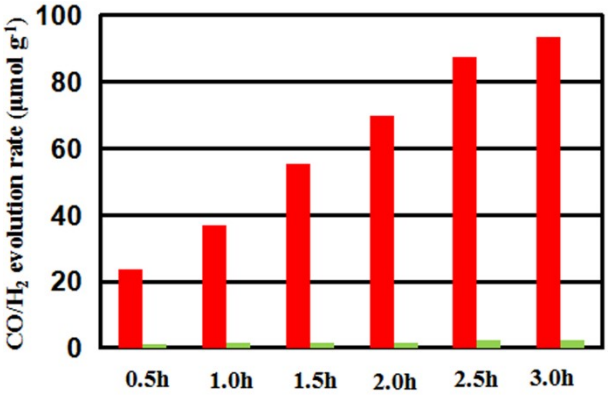

Fig. S7 CO (red column) and H_2 (green column) formation rates of UiO-66-NH_2 at given times.

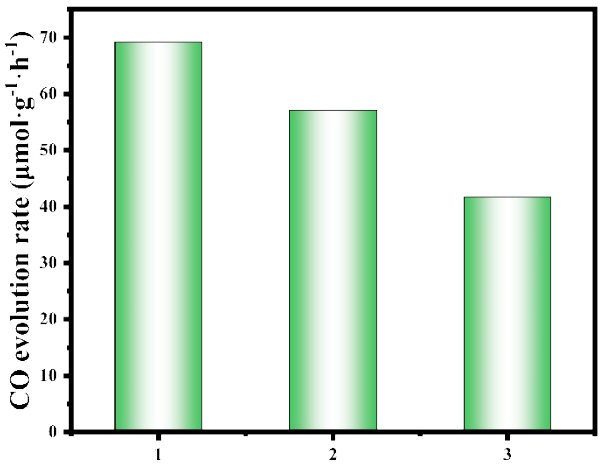

Fig. S8 The cycling stability of UiO-66-NH_2 in CO_2 photocatalytic reduction experiment.

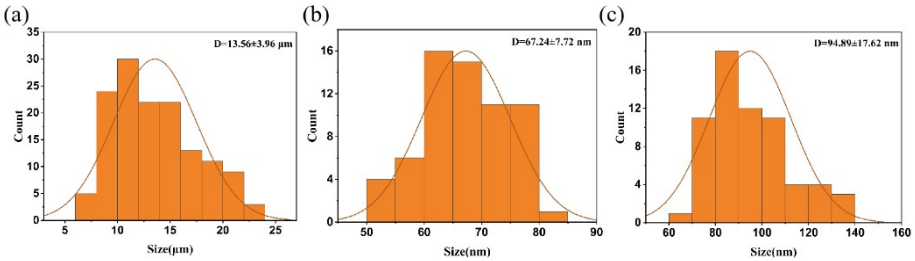

Fig. S9 Particle size charts of (a) BUiO-66-NH_2, (b) AUiO-66-NH_2 and (c) UiO-66-NH_2.

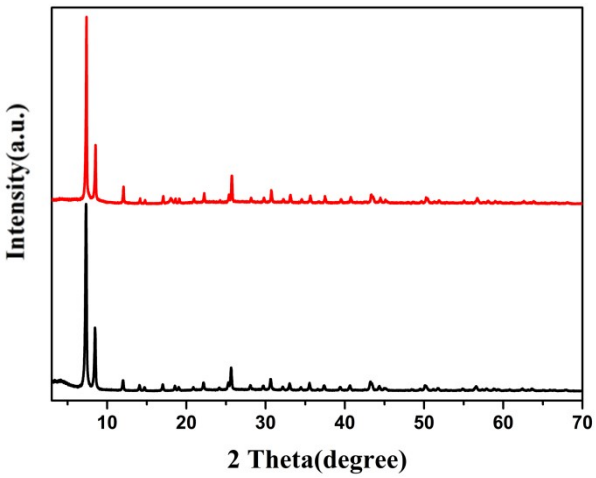

Fig. S10 The PXRD patterns of UiO-66-NH_2 before (black line) and after (red line) photocatalysis.

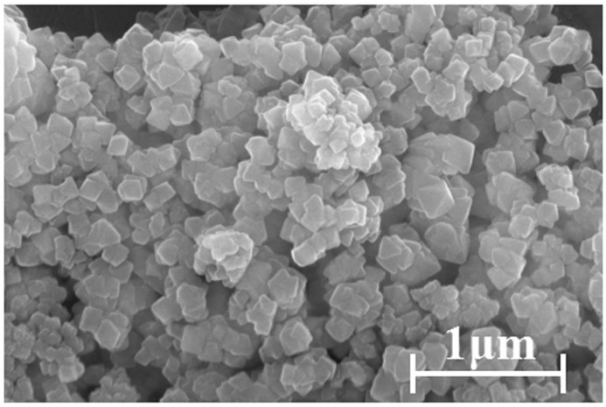

Fig. S11 The SEM image of UiO-66-NH_2 after photocatalysis.

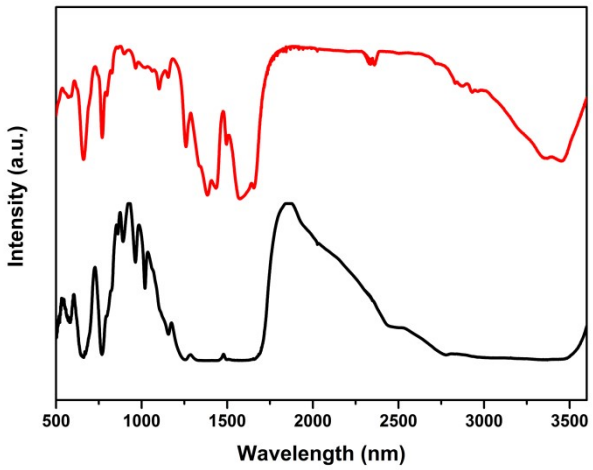

Fig. S12 The FT-IR spectrum of UiO-66-NH_2 before (black line) and after photocatalysis (red line).

Reference

S1 B. Bueken, N. V. Velthoven, T. Willhammar, T. Stassin, I. Stassen, D. A. Keen, G. V. Baron, J. F. M. Denayer, R. Ameloot, S. Bals, D. De Vos and T. D. Bennett, *Chem. Sci.*, 2017, **8**, 3939-3948.

S2 N. Assaad, G. Sabeh and M. Hmadeh, *ACS Appl. Nano Mater.*, 2020, **3**, 8997-9008.

S3 G. Wu, J. Ma, S. Li, S. Wang, B. Jiang, S. Luo, J. Li, X. Wang, Y. Guan and L. Chen, *Environ. Res.*, 2020, **186**, 109542.

S4 M. Cheng, P. Yan, X. Zheng, B. Gao, X. Yan, G. Zhang, X. Cui and Q. Xu, *Chem.*

Eur. J., 2023, **2968**, e202302395.

S5 X.-M. Cheng, X.-Y. Dao, S.-Q. Wang, J. Zhao and W.-Y. Sun, *ACS Catal.*, 2021, **112**, 650-658.

S6 Y. Liu, C. Chen, J. Valdez, D. Motta Meira, W. He, Y. Wang, C. Harnagea, Q. Lu, T. Guner, H. Wang, C.-H. Liu, Q. Zhang, S. Huang, A. Yurtsever, M. Chaker and D. Ma, *Nat. Commun.*, 2021, **121**, 1231.

S7 L. Chen, Q. Liu, J. Yang, Y. Li and G. Li, *Chin. Chem. Lett.*, 2023, **342**, 107335.

S8 T. Wei, L. Wang, K. Mao, J. Chen, J. Dai, Z. Zhang, L. Liu and X. Wu, *J. Colloid Interface Sci.*, 2022, **622**, 402-409.

S9 H. Yang, C. Lai, M. Wu, S. Wang, Y. Xia, F. Pan, K. Lv and L. Wen, *Chem. Eng. J.*, 2023, **455**, 140425.

S10 X. Lu, J. Qian, X. Yuan, Y. Lu, J. Sun, H. Zheng and C. Zhang, *Cryst. Growth Des.*, 2023, **239**, 6719-6724.

S11 Z.-H. Zhou, X.-B. Li, Z.-W. Huang, Q.-Y. Wu, J.-X. Wang, Z.-H. Zhang, J.-P. Yu, L. Mei, F.-Q. Ma, K.-Q. Hu and W.-Q. Shi, *Inorg. Chem. Front.*, 2024, **11**, 6493-6501.

S12 K. Song, S. Liang, X. Zhong, M. Wang, X. Mo, X. Lei and Z. Lin, *Appl. Catal., B*, 2022, **309**, 121232.

S13 J. Zhang, Y. Wang, H. Wang, D. Zhong and T. Lu, *Chin. Chem. Lett.*, 2022, **334**, 2065-2068.

S14 Z.-Y. Du, Y.-Z. Yu, N.-F. Li, Y.-S. Xue, L.-X. Xu, H. Mei and Y. Xu, *Sustain. Energy Fuels*, 2021, **515**, 3876-3883.

S15 J. Nai, S. Wang and X. W. Lou, *Sci. Adv.*, 2019, **5**, 5095.

S16 Z.-B. Fang, T.-T. Liu, J. Liu, S. Jin, X.-P. Wu, X.-Q. Gong, K. Wang, Q. Yin, T.-F. Liu, R. Cao and H.-C. Zhou, *J. Am. Chem. Soc.*, 2020, **14228**, 12515-12523.

S17 N.-Y. Huang, J.-Q. Shen, X.-W. Zhang, P.-Q. Liao, J.-P. Zhang and X.-M. Chen, *J. Am. Chem. Soc.*, 2022, **14419**, 8676-8682.

S18 Y. Han, H. Xu, Y. Su, Z.-l. Xu, K. Wang and W. Wang, *J. Catal.*, 2019, **370**, 70-78.

S19 Y. Xie, Z. Fang, L. Li, H. Yang and T.-F. Liu, *ACS Appl. Mater.*, 2019, **1130**,

27017-27023.